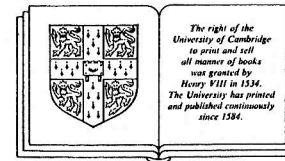


# Physics and chemistry of the upper atmosphere

M. H. Rees

*University of Alaska, Fairbanks*



CAMBRIDGE UNIVERSITY PRESS  
Cambridge  
New York Port Chester Melbourne Sydney

---

## An Overview

### 1.1 Introduction

The definition of the term 'upper atmosphere' is not agreed upon by all scientists. To meteorologists it usually refers to the entire region above the troposphere, where the daily weather evolves. With this interpretation the upper atmosphere would include the stratosphere, mesosphere, and thermosphere, regions identified by their temperature structure, density, composition and the degree of ionization. Figure 1.1.1 illustrates schematically the altitude variation of these atmospheric parameters. Logarithmic scales are used for the abscissae and the ordinate to accommodate the large range of densities and heights.

The same laws of physics apply throughout the atmosphere, of course, but the relative importance of various processes varies widely between regions, accounting for the different behaviour of the characteristic parameters as a function of altitude. Thus, the temperature structure is governed by the absorption of solar radiation, and different wavelength bands are absorbed by various constituents in the region. For example, absorption by  $O_3$  specifically accounts for heating in the stratosphere. Radiation transfer and terrestrial albedo also contribute to the temperature structure. Each region identified in Figure 1.1.1 warrants a book length treatment. In this work we study that portion of the upper atmosphere labelled the thermosphere and ionosphere.

For centuries, man's perception of the thermosphere was limited to the splendour of the Aurorae Borealis and Australis. It was the need for the propagation of radio waves over long distances that provided a practical stimulus to investigations of the thermosphere and the physical processes that cause and control the ionosphere. Compared with the density of the atmosphere at the Earth's surface, the thermosphere is a very high vacuum indeed, but not so perfect as to preclude drag and perturbations on satellites orbiting within the region. The need to predict thermospheric and ionospheric variability has arrived with the space age.

The region where

- (1) energy input is dominated by solar ultraviolet (UV) photons and auroral energetic particles, electric fields and electric currents;

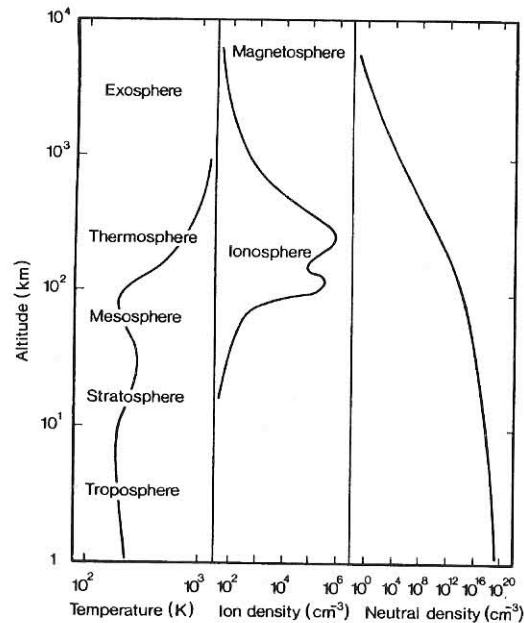


Fig. 1.1.1 Schematic representation of the thermal structure, the ion density and the neutral density of the Earth's atmosphere. The approximate altitude regimes of various named regions are indicated.

- (2) the major neutral constituents are  $O$ ,  $N_2$  and  $O_2$ , and the minor constituents are  $NO$ ,  $N$ ,  $H$ ,  $He$ ,  $Ar$  and  $CO_2$ ; and
- (3) neutral atmosphere dynamics are strongly influenced by plasma motions

is identified as the thermosphere. It is, however, unrealistic to define precisely the boundaries of this region since the three characteristics are not sharply confined in altitude. For example, a small fraction of the UV radiation as well as high energy charged particles penetrate to lower levels in the atmosphere.

While it is possible to identify a region for the purpose of detailed study, nature does not allow us to decouple the region from its neighbours. Thus, the thermosphere is coupled energetically, dynamically, and chemically to the mesosphere at its lower bound, and to the exosphere and magnetosphere at its upper bound. Escape of gas becomes a dominant process in the exosphere, while the degree of ionization becomes high in the magnetosphere and the motion of ions is no longer dominated by collisions with the neutral gas. The complexity of neutral and ion chemistry increases substantially in the mesosphere due to a host of minor constituents, both neutrals and ions, the formation of large molecules, and influences propagating up from the troposphere.

There is one attribute that distinguishes the thermosphere from its neighbours, above and below. It is the region where most radiations from the atmospheric atoms and molecules in the visible spectrum originate, i.e., the nightglow, the dayglow and the aurora. All three phenomena are visible from a space platform. The nightglow is

generally too faint and structureless to be seen by the naked eye from the ground while the dayglow is overwhelmed by scattered sunlight in the lower atmosphere. The aurora is the visual manifestation of processes that we shall study in detail in subsequent chapters.

Instruments have been developed that are capable of measuring such radiation from the upper atmosphere. Analysis of various emission features has yielded insight into chemical processes, energy balance and the dynamic behaviour of the upper atmosphere. This has been accomplished by passive remote sensing, i.e., without perturbing the medium or process under study. Radar techniques have been used extensively to investigate the properties and behaviour of the ionized component of the thermosphere and to derive several important dynamical and compositional properties of the region. Direct, *in situ* measurements by rocket and satellite borne instruments have provided a wealth of data on the composition, structure, and dynamics of the upper atmosphere over a wide range of altitude and large geographic extent. Many instruments and widely different experimental methods that are complementary have been adopted to make observations of and collect measurements about the thermosphere, thus providing inputs to models which, ultimately, will test our understanding of one part of our environment.

## 1.2 Physical properties of the upper atmosphere

An appreciation of the complexity of the physics and chemistry of the upper atmosphere may be acquired by listing the various processes that occur simultaneously and the resulting observable quantities. Adopting the organization that will be followed in succeeding chapters we identify processes with the basic conservation laws of physics, as shown in Figure 1.2.1, noting that the various processes and their mathematical descriptions are coupled.

*Atmospheric composition:* The neutral composition of the thermosphere is governed to a large extent by the evolution of the planet, a topic that is outside the scope of this text. Thus, processes that establish the abundance of  $N_2$ ,  $O_2$ ,  $Ar$ ,  $He$ ,  $H$  and  $CO_2$  are not considered. We are interested in  $O$  because it is produced by photodissociation and energetic particle impact dissociation. We are also interested in the minor species,  $N$  and  $NO$ , produced by molecular dissociation and various chemical reactions.

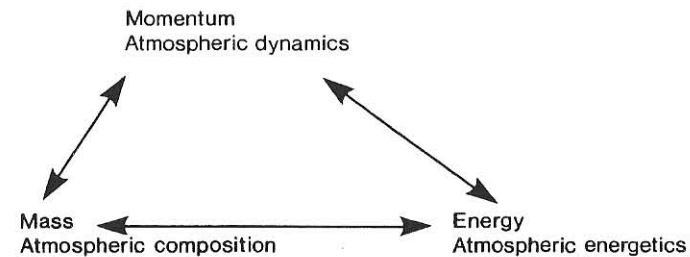


Fig. 1.2.1 Coupling between atmospheric composition, energetics and dynamics by the conservation laws of physics.



Of special interest are atoms and molecules in excited states producing the optical emissions that are the signature of important processes in the upper atmosphere. (The term 'optical emissions' includes radiation in the visible as well as the UV and infrared (IR) regions of the spectrum.) Excited state atoms and molecules are produced by UV photon impact as well as charged particle impact collisions and by subsequent chemical reactions. The minor neutral composition and the excited state production are closely related to the ion production and composition. UV and particle impact ionization of the major thermospheric species,  $N_2$ ,  $O_2$ , and  $O$ , initiates a chain of ion chemistry reactions that determine the time-varying ion composition and abundance. Thus, while NO molecules are only a minor neutral species in the thermosphere, as a result of the ion chemistry  $NO^+$  ions are a major constituent in the E- and lower F- regions of the ionosphere. The typical ion density–height profile in the centre panel of Figure 1.1.1 shows that the ion density occurs in layers.

*Atmospheric dynamics:* The thermosphere and ionosphere form a dynamic system that responds to a variety of forces or momentum sources. Diurnal and latitudinal variations of neutral gas heating cause pressure gradients which, together with the Coriolis effect, force zonal and meridional winds. Ions are driven by electric fields causing them to convect from one region of the ionosphere to another, constrained by the Earth's magnetic field. Collisions between ions and neutrals couple their motion so that ion drag participates in establishing the pattern of the winds. The resulting velocity vectors are asymmetric over the globe because the electric field configuration is governed by the geomagnetic field, whose poles are displaced from the geographic poles, while the Coriolis effect depends on the rotational symmetry of the Earth.

Vertical motion is governed largely by gravitational acceleration and pressure gradients. Molecular diffusion causes the density of individual neutral constituents to vary independently with altitude. The effect becomes important above about 120 km, resulting in a rapid decrease in the densities of heavier molecular species with altitude compared with the lighter atomic species. Another process that occurs in the atmosphere is turbulence which causes small scale eddy motions that are embedded in the large scale mean motion characterized by winds. Turbulence can be produced by thermal gradients and by wind shear, both effects existing in the lower thermosphere. Transport of the small eddies results in turbulent diffusion which tends to smooth out differences between air parcels and maintain a mixed gas. The effect dominates below 100 km. In addition to the effects of an externally applied electric field, ions are subject to dynamo action when driven by the neutral wind in the geomagnetic field.

*Atmospheric energetics:* The interaction of solar UV photons and energetic particles with the thermosphere and ionosphere is a source of heat for the neutral and ionized constituents. Ionospheric currents driven by electric fields cause frictional heating of the neutrals and ions that is a major energy source at high latitudes. Thus, differential motion between the neutral and ionized species is both a momentum and an energy source for the upper atmosphere.

While energetic photons and particles are the carriers of energy, direct collisional transfer of energy to the atmosphere is small by comparison with indirect heating by exothermic chemical and ionic reactions. Photoionization and dissociation, and electron impact ionization and dissociation, produce ions and atoms that may be

converted to different species and that eventually recombine. The most likely reactions are exothermic, resulting in the conversion of photon and electron energy into kinetic energy of the neutral and ionized gas. These are the processes that yield the observed temperature variation with altitude. A small fraction of the energy absorbed in the thermosphere is radiated to space or to lower levels of the atmosphere and to the ground. The radiation is in the form of spectral features, i.e., atomic lines, molecular bands and recombination continua that originate from numerous excited states of several species.

Interdependence between composition, dynamics, and energetics emerges from the descriptive presentation given in the preceding paragraphs. The coupled nature of the problem is also demonstrated by its mathematical formulation.

Unlike lower levels of the atmosphere, the constituents of the thermosphere are not fully mixed. It becomes necessary, therefore, to describe the behaviour of each species by its own continuity, momentum and energy equations. Each species has its own production and loss rates, transport properties and thermal characteristics, and is subject to different forces. However, there is also interaction between the constituents through collisional processes involving momentum and energy transfer as well as chemical reactions, and through electromagnetic and gravitational forces.

The concentration of the  $j$ th constituent,  $n_j$ , is given by the continuity equation,

$$\partial n_j / \partial t + \nabla \cdot (n_j \mathbf{v}_j) = P_j - L_j \quad (1.2.1)$$

where  $P_j$  and  $L_j$  are the production and loss rates and  $\mathbf{v}_j$  is the velocity vector. Each term in the continuity equation represents a rate of change of the concentration of species  $j$  per unit volume with time,  $t$ . The second term on the left side of Equation (1.2.1) represents the flux divergence.

Motion of the  $j$ th constituent is given by the momentum equation,

$$\rho_j D_j \mathbf{v}_j / Dt + \nabla \cdot \bar{\mathbf{P}}_j = \sum_j n_j \mathbf{F}_j \quad (1.2.2)$$

The inertial term and the generalized pressure tensor term on the left side of the equation are balanced by the external forces,  $\mathbf{F}_j$ , on the right side.  $\rho_j$  is the mass density,  $\bar{\mathbf{P}}_j$  is the pressure tensor and the external forces are gravitational and electromagnetic. (The convective derivative is  $D_j / Dt = \partial / \partial t + \mathbf{v}_j \cdot \nabla$ .) Each term in the momentum equation represents a force per unit volume.

The thermal properties are specified by the energy equation,

$$n_j k D_j T_j / Dt = Q_j - L_j^T - n_j k T_j \nabla \cdot \mathbf{v}_j - \nabla \cdot \mathbf{q}_j + \sum_j n_j \mathbf{F}_j \cdot \mathbf{v}_j \quad (1.2.3)$$

Each term represents a time rate of change of energy per unit volume. The net rate of change (left side of the equation) is equal to the sum of the local heating rate,  $Q_j$ , heat loss rate,  $L_j^T$ , compressional heating (or cooling), divergence of the heat flow,  $\mathbf{q}_j$ , and the work done on species  $j$ .

The equation of state

$$p_j = n_j k T_j \quad (1.2.4)$$

relates parameters that appear in the three conservation equations and defines the partial pressure of the  $j$ th species;  $k$  is Boltzmann's constant. At the temperatures that



prevail in the upper atmosphere the macroscopic properties of the gas obey Boltzmann statistics and the energy of the system can be described by classical mechanics. The ideal gas law (Equation (1.2.4)) is therefore an appropriate equation of state. In the upper atmosphere the transfer of molecular properties can be analysed by a set of transport equations. Particle motion is specified in terms of a distribution function in phase space and a flux vector is associated with each macroscopic property. The distribution function incorporates streaming and external forces. Including interactions amongst the particles of the system, collisions, leads to the Boltzmann equation for the distribution. Moments of the distribution function yield the transport properties; the first three correspond to the transport of mass, momentum, and kinetic energy, the conservation equations (Equations (1.2.1), (1.2.2) and (1.2.3)).

Application of the conservation laws to the various neutral and ion species yields the height profiles of the respective concentrations and temperatures, as well as the wind fields. However, the development of three-dimensional time-dependent models of the thermosphere and ionosphere has only recently begun. Even as these words are written, work on this problem is progressing at a rapid pace and the status reported in this book will have been superseded at the time of its publication. We endeavour, therefore, to emphasize the physics and chemistry of the basic processes that occur in the upper atmosphere.

Topics in the succeeding chapters are arranged to thread the following argument. The production and loss mechanisms in the continuity and energy equations,  $Q_j$  and  $L_j^T$ , are the microphysics that underlie the transport phenomena which govern the thermodynamics of the upper atmosphere. We therefore begin with the influence of solar UV radiation and energetic particle bombardment on the composition of the thermosphere and the ionosphere, including subsequent chemical and ionic reactions. This leads us into investigating various energy dissipation mechanisms for the incoming radiations. These include optical emissions that make up the airglow and aurora which are a conspicuous energy sink but only account for a very small fraction of the total energy. By far the largest fraction is dissipated locally, driving the wind system and establishing the temperature profile, our next topic. Ions are driven by electric fields and by the neutral wind. In the upper atmosphere ion and neutral gas motions are coupled, so that the ions become both a momentum and a heat source for the neutrals. Electric fields influence both the dynamics and energetics of the atmosphere. Electric fields drive current systems that provide the link between the ionosphere and the magnetosphere.

The properties of the upper atmosphere that are measured *in situ* or remotely comprise the body of facts from which models are constructed. Even in the 25 years in which the thermosphere has been studied in some detail we have come to realize that the structure and composition of this region is highly variable. This is a consequence of the dynamic behaviour of the atmosphere so that the state at any given time is a function of the preceding state over wide ranging time scales. The atmosphere has a memory and is continually evolving. Evolution of the atmosphere on geologic time scales is a book length topic by itself and will not be dealt with here (see references at the end of the chapter). The longest time scale that we will consider is related to the systematic variability of solar UV photon and energetic particle emission over an 11 year cycle of solar activity, commonly measured by the sunspot number. This variability is sufficient to produce significant changes in thermospheric parameters and

thereby furnish a starting point in delineating the processes that determine its properties. Thus, the temperature and density profiles shown in Figure 1.1.1 are illustrative and typical but do not refer to a specific situation. There are significant systematic diurnal, seasonal, and positional (both geographic and geomagnetic) variations in density and temperature. By contrast, variations associated with the fluctuating solar wind are large and more difficult to predict. A quantitative description of thermospheric and ionospheric structure, dynamics and energetics therefore requires time-dependent solutions of the governing equations.

We shall not stray far from observable quantities throughout this work. Indeed, the analyses will be guided by them. The relative importance of various processes, however, changes markedly for different observables. For example, understanding the origin of certain auroral optical radiations requires only solution of a one-dimensional transport equation for electrons, with a measured initial phase space distribution function, and application of the excited state chemistry of some ionic and neutral species. Of much greater complexity is the modelling of the global neutral wind system which involves a coupled three-dimensional solution of all the conservation equations.

## Bibliography

- The physical and chemical processes to which the Earth's atmosphere has been subjected in the geologic past, leading to its present composition, are described in  
 J.C.G. Walker, *Evolution of the Atmosphere*, Collier Macmillan Publ. Co., New York, 1977.  
 A. Henderson-Sellers, *The Origin and Evolution of Planetary Atmospheres*, Adam Hilger Ltd., Bristol, 1983.



## The interaction of energetic solar photons with the upper atmosphere

The major neutral molecular constituents in the thermosphere,  $N_2$  and  $O_2$ , are a legacy of the evolution of the Earth's atmosphere, and the present day abundance is controlled largely by geochemical and biological processes, as is the concentration of the minor molecular species,  $CO_2$ . The major atomic constituent,  $O$ , is produced from dissociation of  $O_2$  by solar UV photons and by energetic particle impact. These processes also account for the presence of  $N$  atoms. The minor species  $NO$ ,  $O_3$  and  $OH$  result from chemical reactions, while  $H_2O$ ,  $He$ ,  $H_2$ ,  $Ar$ ,  $CH_4$  and  $CO_2$  are transported into the thermosphere from the mesosphere and lower levels of the atmosphere.

All the charged species that make up the ionosphere are produced either directly by photoionization and impact ionization of neutral atoms and molecules, or indirectly by subsequent ionic-chemical reactions. Photodetachment rapidly destroys any negative ions that may be formed in the thermosphere and the ionic population consists of several species of positive ions and an electron density equal to the sum of the positive ion densities.

In this chapter we compute the direct production rates of  $O$  and  $N$  atoms, and of the ions  $N_2^+$ ,  $O_2^+$ ,  $N^+$  and  $O^+$  by energetic photons. This requires knowledge of the energy distribution of the solar UV intensity, various cross sections (defined in Chapter 4), and densities of the major molecular species. Electronically excited states of atoms, molecules and ions will be treated because excited states play a major role in chemical reactions, spectroscopic emissions, and the energy balance in the thermosphere.

### 2.1 The solar irradiance

The transfer of solar radiation in the atmosphere does not involve emission sources or scattering into the original beam (with some important exceptions that are taken up in Chapter 7), and the process is well described by the Lambert-Beer exponential absorption law,

$$I(\lambda) = I_{\infty}(\lambda) \exp[-\tau(\lambda)] \quad (2.1.1)$$

At any point in the atmosphere the intensity at wavelength  $\lambda$  is  $I(\lambda)$  and  $\tau(\lambda)$  is the optical depth. In this section we focus on the irradiance at 1 AU 'at the top of the

atmosphere', i.e.,  $I_{\infty}(\lambda)$ . The optical depth will be taken up in Section 2.2.

The wavelength region with which we concern ourselves is the UV portion of the solar spectrum which is absorbed in the atmosphere above about 80 km. Space borne instruments are therefore required to measure the radiation and this has only become possible since the advent of rocket and satellite technology. Solar UV irradiance measurements extend over solar cycle 20 and, to date, about half of cycle 21. Measurements made with instruments carried on board satellites yield data over extended periods of time but the inability to perform in-flight calibration and the inevitable degradation of detectors lead to uncertainties in both absolute and relative values of the irradiance at different wavelengths. Rocket borne instruments yield snapshots of the solar irradiance, but less than two dozen measurements have been made since 1960, most experiments covering only a limited wavelength interval. Even the limited data sets that have been obtained clearly show considerable variability in the UV spectral intensities, with the magnitude of the variability related to other variable solar parameters such as the decametric radiation, cyclical variations, and flare activity.

The solar UV spectrum between 14 Å and 2000 Å obtained on 23 April 1974 is shown in Figure 2.1.1. The wavelength resolution is 1 Å and the flux magnitude, usually specified in units of photons  $cm^{-2} s^{-1} \text{Å}^{-1}$ , is just photons  $cm^{-2} s^{-1}$  in this case. This

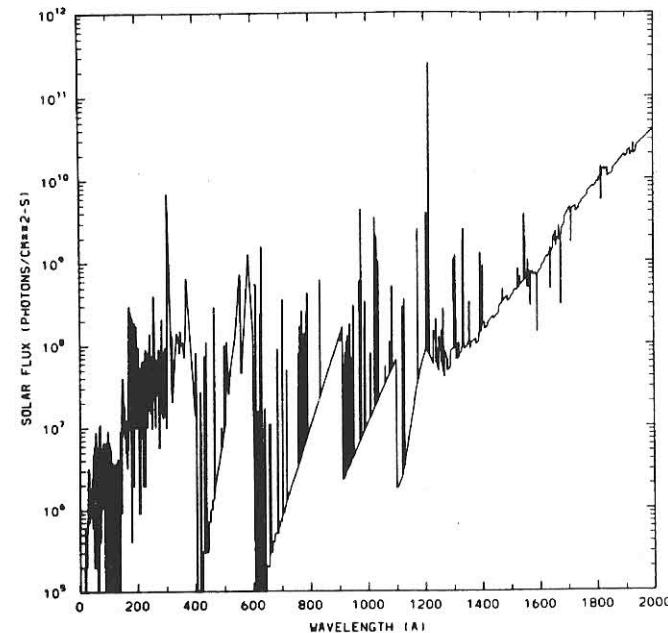


Fig. 2.1.1 Solar UV flux measured on 23 April 1974 at 1 Å intervals. This is the aeronautical reference spectrum F74113 for the Atmosphere Explorer satellite solar flux measurements. (R.G. Roble and B.A. Emery, *Planet. Space Sci.*, 31, 597, 1983.)

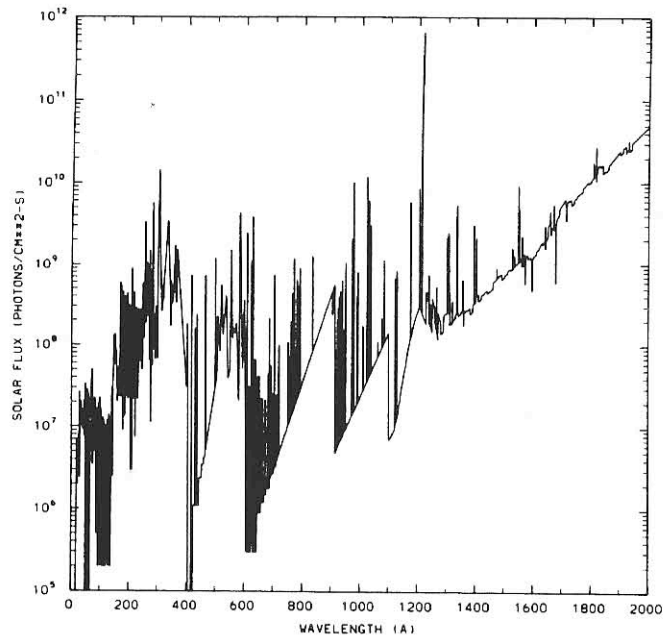


Fig. 2.1.2 Solar UV flux measured on 19 February 1979 at 1 Å intervals. (R.G. Roble and B.A. Emery, *Planet. Space Sci.*, 31, 597, 1983.)

is an important spectrum because it served as a calibration spectrum for the spectrometers carried by the Atmosphere Explorer satellites between 1974 and 1981. The April 1974 epoch is representative of solar minimum activity. Figure 2.1.2 shows a similar spectrum obtained five years later during the maximum of the solar activity cycle. A brief period in July 1976, during which there were essentially no sunspots on the disc, is adopted as representative of minimum solar UV irradiance. The ratio of the solar UV flux obtained on 19 February 1979 to the July 1976 minimum is shown in Figure 2.1.3. The solar UV irradiance spectrum is a composite of many emission lines and continua (Problem 1). The flux varies over many orders of magnitude in the wavelength interval that contributes to thermospheric and ionospheric processes. Flux variability between solar maximum and solar minimum conditions strongly depends on wavelength. Variability is largest at the short wavelengths consisting of emission from the hottest region of the solar atmosphere, the corona and the upper chromosphere. Large increases of irradiance are associated with solar flares. Geophysical parameters associated with the April 1974, July 1976 and February 1979 periods are summarized in Table 2.1.1.

The pictorial presentation of the solar UV irradiance (Figures 2.1.1–2.1.3) provides a good overview of the wavelength dependence of this input parameter. However, for computations it is more convenient to present the measurements in tabular form and to combine photon intensities into larger wavelength intervals. Intensities of the brighter

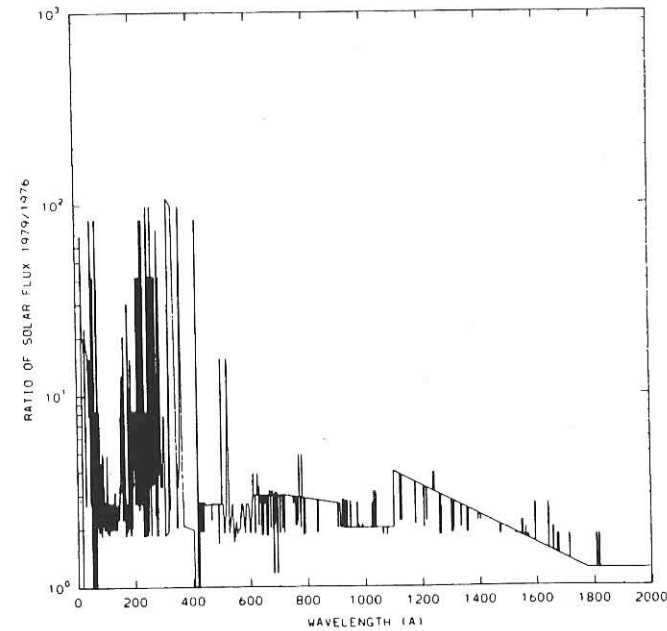


Fig. 2.1.3 Ratio of solar UV intensities measured on 19 February 1979 to the observations obtained during July 1976 on days of spotless solar conditions. (R.G. Roble and B.A. Emery, *Planet. Space Sci.*, 31, 597, 1983.)

Table 2.1.1 Geophysical parameters for various periods

Day	F 10.7	$\bar{F} 10.7$	$E_r$	$A_p$	$K_p$
23 April 1974	74.5	86.1	1.99	29	5 <sup>-</sup> 4 <sup>-</sup> 4 <sup>-</sup> 5 <sup>-</sup> 4 <sup>-</sup> 4 <sup>-</sup>
13–28 July 1976	66.4–69.1	71.8	2.07	3–19	1 <sup>-</sup> 1 <sup>-</sup> 0 <sup>-</sup> 1 <sup>-</sup> 2 <sup>-</sup> 1 <sup>-</sup> 0 <sup>-</sup> (21 st)
	(average = 67.6)		(average = 7)	(15th)	2 <sup>-</sup> 2 <sup>-</sup> 2 <sup>-</sup> 2 <sup>-</sup> 2 <sup>-</sup> 4 <sup>-</sup> 6 <sup>-</sup>
19 February 1979	243.3	187.7	7.19	15	4 <sup>+</sup> 3 <sup>+</sup> 3 <sup>+</sup> 2 <sup>+</sup> 4 <sup>+</sup> 2 <sup>+</sup> 3 <sup>+</sup>

F 10.7 – the 10.7 cm radiowave flux from the sun in units of ( $\times 10^{-22} \text{ W m}^{-2} \text{ Hz}^{-1}$ ) for the previous day.

$\bar{F} 10.7$  – the 3 month solar rotation average of the F 10.7 solar flux centred on the day indicated.

$E_r$  = solar UV energy flux in  $\text{erg cm}^{-2} \text{ s}^{-1}$  integrated in wavelength from 14.25 to 1017 Å.

$A_p$  = daily planetary geomagnetic index.

$K_p$  = three hourly values of the planetary magnetic index on a quasi-logarithmic scale ranging from 0 to 9<sup>+</sup>.

emission lines are still listed separately. One such tabulation is shown in Appendix 2 for five representative days in solar cycle 20. The wavelength range between 50 and 1050 Å includes the ionization energy of all major atomic and molecular constituents of the thermosphere (Section 2.3). Longer wavelength photons are capable of dissociating  $\text{O}_2$  molecules, as well as other species; this will be discussed in Section 2.4. The reference



spectrum in the wavelength range between 1050 and 1940 Å is listed in Appendix 2. Considerable variability of the solar irradiance is still found in this wavelength region, as shown in Figure 2.1.3.

## 2.2 The optical depth

The optical depth,  $\tau(\lambda)$ , a parameter that appears in the Lambert-Beer law (Equation (2.1.1)), specifies the attenuation of the solar irradiance by the atmosphere. For a vertical sun, and at altitude  $z_0$  it is, simply,

$$\tau_{z_0}^v(\lambda) = \sum_j \sigma_j^a(\lambda) \int_{z_0}^{\infty} n_j(z) dz \quad (2.2.1)$$

where the  $\sigma_j^a(\lambda)$ s are the wavelength-dependent absorption cross sections of species  $j$  and the  $n_j(z)$ s are the height profiles of their concentrations. For a slant path on a spherical earth the equation is slightly more complex. Figure 2.2.1 illustrates the geometry for solar zenith angles  $\chi_0$  less than  $90^\circ$  and greater than  $90^\circ$ . The earth's radius is  $R$ , the altitude at which the photon flux is evaluated is  $z_0$ , and  $z_s$  is a screening height below which the atmosphere is essentially opaque to photons of wavelength  $\lambda$ . For the  $\chi_0 < 90^\circ$  case,

$$\frac{\sin \chi}{R + z_0} = \frac{\sin \chi_0}{R + z} \quad (2.2.2)$$

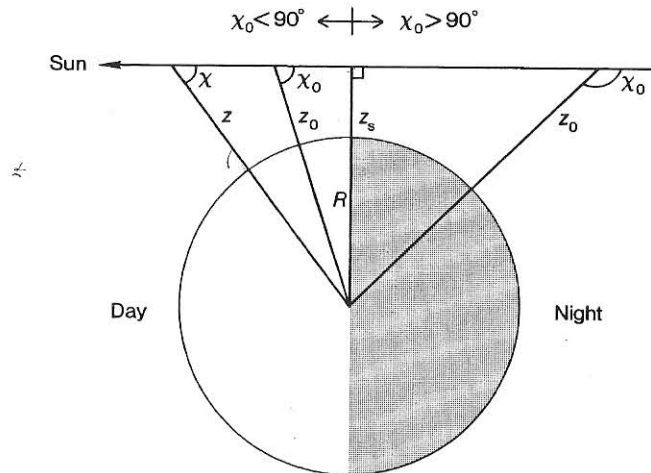


Fig. 2.2.1 Geometry adopted for computing the attenuation of solar irradiance (not to scale).

from which

$$\sec \chi = \left[ 1 - \left( \frac{R + z_0}{R + z} \right)^2 \sin^2 \chi_0 \right]^{-1/2} \quad (2.2.3)$$

and the optical depth is

$$\tau(\lambda, \chi_0, z_0) = \sum_j \sigma_j^a(\lambda) \int_{z_0}^{\infty} n_j(z) \left[ 1 - \left( \frac{R + z_0}{R + z} \right)^2 \sin^2 \chi_0 \right]^{-1/2} dz \quad (2.2.4)$$

Substantial effort has been devoted in the past toward expressing the integral by some analytic function, generically known as the Chapman function, or in tabular form. This hardly seems necessary any longer considering the ease of obtaining a solution numerically using a computer. For a solar zenith angle  $\chi_0$  less than about  $75^\circ$  it is found that  $\sec \chi \approx \sec \chi_0$  for values of  $z_0$  corresponding to ionospheric levels. The integral must still be retained if the altitude profiles of the concentrations of various species are arbitrary and not expressed in some analytic form.

For a solar zenith angle  $\chi_0 > 90^\circ$  the optical depth is

$$\tau(\lambda, z_0, \chi_0) = \sum_j \sigma_j^a(\lambda) \left\{ 2 \int_{z_s}^{\infty} n_j(z) \left[ 1 - \left( \frac{R + z_s}{R + z} \right)^2 \right]^{-1/2} dz - \int_{z_0}^{\infty} n_j(z) \left[ 1 - \left( \frac{R + z_0}{R + z} \right)^2 \sin^2 \chi_0 \right]^{-1/2} dz \right\} \quad (2.2.5)$$

The derivation is left as a problem (Problem 2). When  $\chi_0 = 90^\circ$  Equation (2.2.5) reduces to Equation (2.2.4) since  $z_0 = z_s$ , and for  $\chi_0 = 0^\circ$ , an overhead sun, both Equation (2.2.4) and Equation (2.2.5) reduce to Equation (2.2.1).

The altitude dependence of the concentrations of the major thermospheric neutral species (together with the temperature profile) is known as a neutral atmosphere model. Several empirical models have been developed based on measurements obtained over long periods of time, a range of altitudes, latitudes, longitudes and levels of 'solar activity'. One goal of upper atmosphere research has been, and still is, to test our ability to model the response of the thermosphere and ionosphere to various inputs, such as a variable solar irradiance, i.e., to predict the changes in density, composition, temperature, etc. that are observed. Here we are faced with a dilemma. We must assume a model atmosphere to compute the optical depth which then enables us to derive the solar flux as a function of altitude and the multitude of effects that it has on the atmosphere. Among these effects will be changes in the model parameters that were assumed to begin the process. Moreover, rocket and satellite borne instruments do not measure the solar irradiance at the 'top of the atmosphere'; instead,  $I(\lambda)$  is measured over a range of altitudes. To infer  $I_\infty(\lambda)$  from the measurements a model atmosphere must be assumed. This interdependence of physical parameters is characteristic of the system being studied, the upper atmosphere, and we will be faced with similar situations throughout this book. Appendix 1 is devoted to empirical neutral atmosphere models.

The remaining parameter in the expression for the optical depth is the absorptor cross section. The photoabsorption cross sections for the major thermospheric species are shown in Figures 2.2.2-2.2.4. The wavelength region relevant to our purpose computing ionization and dissociation rates, is determined by the following relation



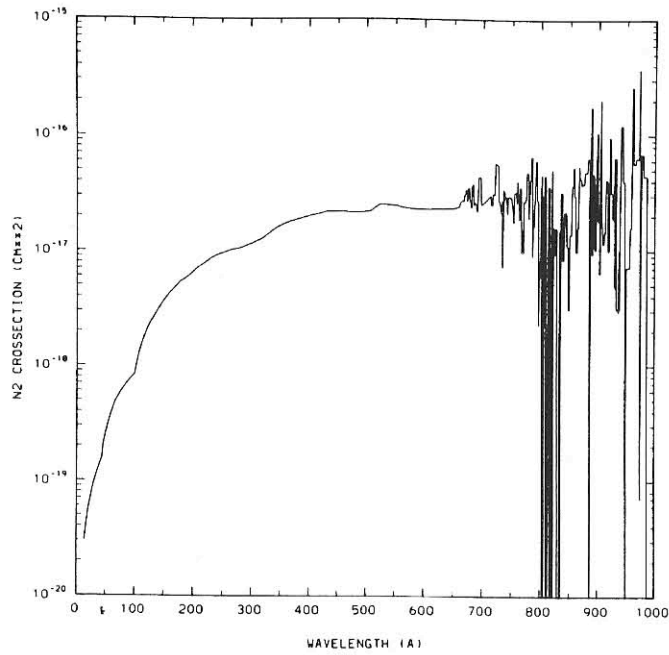


Fig. 2.2.2 Absorption cross sections for  $N_2$ . (R.G. Roble and B.A. Emery, *Planet. Space Sci.*, 31, 597, 1983.)

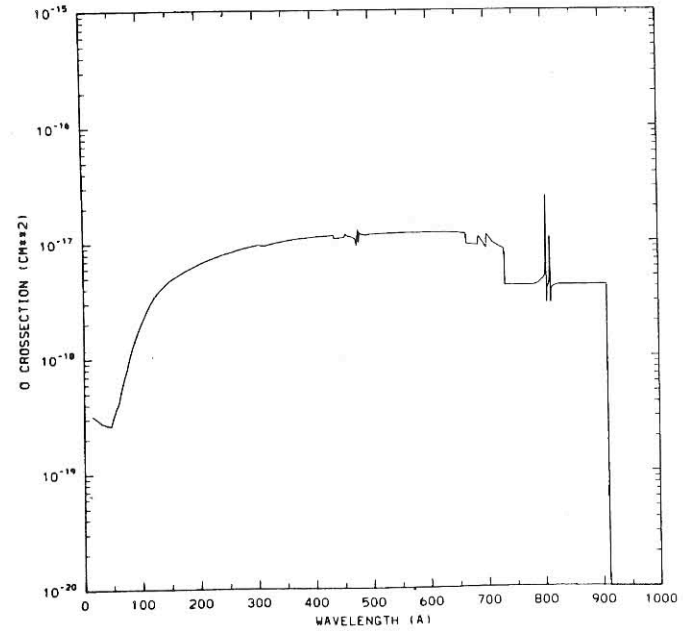


Fig. 2.2.4 Absorption cross sections for O. (R.G. Roble and B.A. Emery, *Planet. Space Sci.*, 31, 597, 1983.)

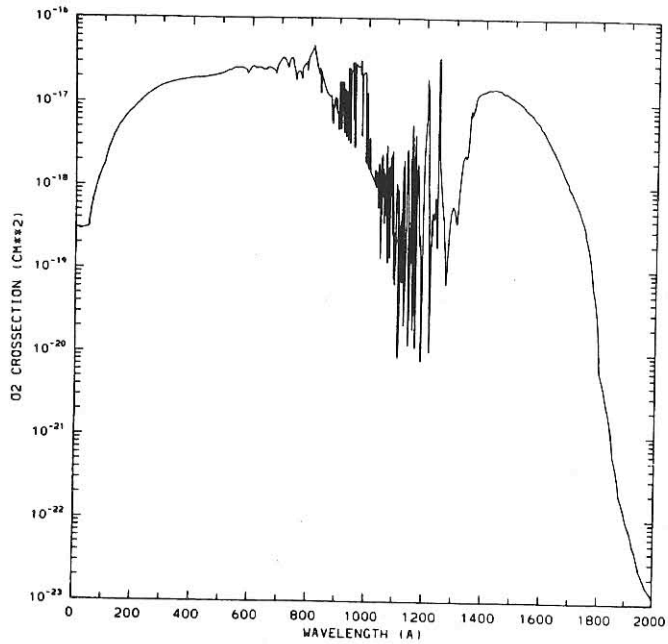


Fig. 2.2.3 Absorption cross sections for  $O_2$ . (R.G. Roble and B.A. Emery, *Planet. Space Sci.*, 31, 597, 1983.)

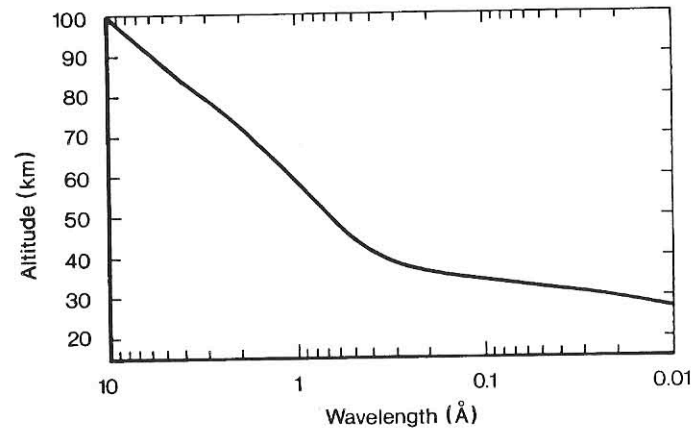


Fig. 2.2.5 Altitudes of the unit optical depth for  $0.01 \leq \lambda \leq 10 \text{ \AA}$ .

Table 2.2.1 Ionization and dissociation threshold energies and wavelengths

Species	Ionization		Dissociation	
	(eV)	$\lambda(\text{\AA})$	(eV)	$\lambda(\text{\AA})$
N <sub>2</sub>	15.58	796	9.76	1270
O <sub>2</sub>	12.08	1026	5.12	2422
O	13.61	911		
N	14.54	853		
NO	9.25	1340	6.51	1905
H	13.59	912		
He	24.58	504		

considerations. The photons must be absorbed in the thermosphere. This implies an absorption cross section which is of the order of magnitude of the inverse of the column density of the absorbing species above the lowest height level of interest, about 90 km, resulting in approximately unit vertical optical depth (Problem 3). Figure 2.2.5 shows the altitude of unit optical depth for X-rays in the wavelength region between 0.01 and 10 Å. The photon energy must also exceed the threshold energy for ionization and/or dissociation of the neutral constituents. Table 2.2.1 presents these thresholds for the thermospheric and ionospheric species. Absorption cross sections are given in tabular form in Appendix 2. Examination of the curves in Figures 2.2.2–2.2.4 shows that in the wavelength region of the continua the absorption cross section varies relatively smoothly with wavelength but that molecular band absorption is highly structured. In the region between the Schumann–Runge continuum and the photoionization limit ( $\sim 1350\text{--}1026\text{ \AA}$ ) in O<sub>2</sub> especially large changes in the magnitude of the cross section occur, varying by three powers of ten within a range of a few angstroms. Fortunately, there is a deep minimum in the absorption cross section ( $\sim 1 \times 10^{-20}\text{ cm}^2$ ) at the wavelength of the H Lyman alpha (H-Ly- $\alpha$ ) solar emission line ( $\sim 1215.7\text{ \AA}$ ) which has a large and variable intensity (Figure 2.2.6). Since this wavelength region lies beyond the absorption edge of O and N<sub>2</sub>, only O<sub>2</sub> need be included in computing the optical depth at 1216 Å. Adopting the O<sub>2</sub> concentration given in Appendix 1 we find that unit optical depth for O<sub>2</sub> is at a level of about 85 km. It would therefore seem that the H-Ly- $\alpha$  radiation should pass right through the thermosphere. This would indeed occur were it not for the minor constituent NO. The ionization threshold wavelength of NO is 1340 Å and the ionization cross section is large. Thus, thermospheric NO is efficiently ionized by H-Ly- $\alpha$ . The NO density, however, is insufficient to prevent most of the radiation from penetrating to the level of the mesosphere and becoming a major source of D-region ionization.

### 2.3 Photoionization

Photoionization is the principal mechanism that produces the ionosphere. For the three major thermospheric species we have

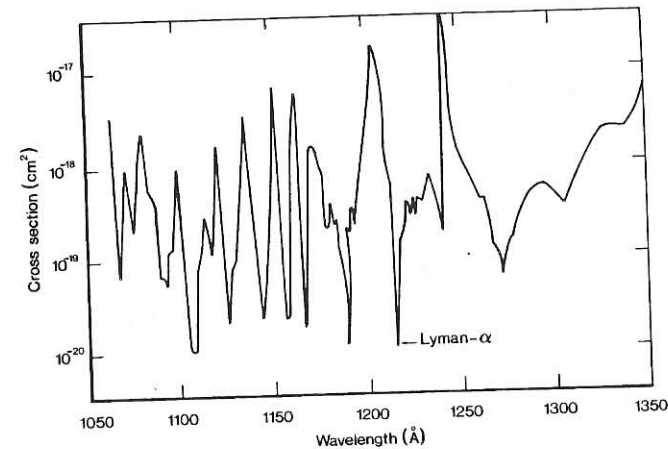
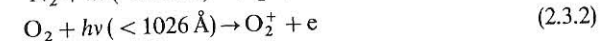
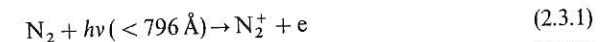
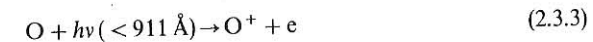


Fig. 2.2.6 Absorption cross sections of O<sub>2</sub> between 1050 and 1350 Å. (K. Watanabe, *Advances in Geophysics*, Eds. H.E. Landsberg and J. Van Mieghen, 5, 153, 1958.)



and



The wavelengths specified in Reactions (2.3.1)–(2.3.3) correspond to the ionization thresholds,  $\lambda_{th}$ , listed in Table 2.2.1 for the production of ions in their ground electronic state. The photoionization rate of species  $j$  at altitude  $z$  is

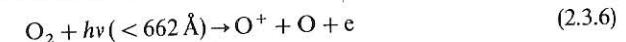
$$P_z^i(j, l) = n_z(j) \int_{\lambda_{th}}^0 I_z(\lambda) \sigma_j^i(\lambda) p_j^i(\lambda, l) d\lambda \quad (\text{ions cm}^{-3} \text{ s}^{-1}) \quad (2.3.4)$$

Quantities not previously defined are the ionization cross section,  $\sigma_j^i(\lambda)$ , and the branching ratios  $p_j^i(\lambda, l)$  that identify production of ions in various electronically excited states,  $l$ , or in the ground state. For each constituent,

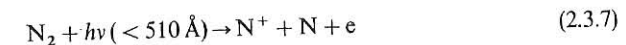
$$\sum_j p_j^i(\lambda, l) = 1 \quad (2.3.5)$$

The integration in Equation (2.3.4) is carried from the ionization threshold wavelength,  $\lambda_{th}$ , to the shortest wavelength (not zero, as has been shown) at which the photon flux is sufficient to contribute to ion production. X-ray photons of wavelength shorter than about 10 Å are absorbed largely below 100 km (Figure 2.2.5). The photon flux is small but highly variable.

Dissociative ionization is an additional source of atomic ions,



and



Photons with sufficient energy to both ionize and dissociate the molecule are required.



The threshold wavelengths for reactions specified up to this point are valid for the formation of ions in the ground state. A substantial fraction of ions and neutrals in the thermosphere is produced in electronically excited states and with an enhanced vibrational population distribution, though the latter not by photon impact. Various consequences of the formation of excited states will be discussed in this and succeeding chapters. An overview of the various states associated with each of the major thermospheric species is best obtained from the energy level diagram for each species. Simplified diagrams showing the excited states of  $N_2^+$ ,  $O_2^+$  and  $O^+$  relevant to the present subject are given in Figure 2.3.1. Complete energy level diagrams for atoms and atomic ions and potential curves as a function of internuclear distance for molecules and molecular ions are presented in Appendix 3; frequent reference will be made to these diagrams. The contribution of double or multiple ionization is too small to warrant inclusion here.

Cross sections for ionization of O leading to different electronic states of the ion have been computed theoretically. For the molecular ions, however, it is difficult both theoretically and experimentally to determine cross sections for each excited ionic state. It has been common practice to specify the total photoionization cross section,  $\sigma_j^i(\lambda)$ , and the branching ratios,  $p_j^i(\lambda, l)$ , using compatible wavelength intervals. The different states of the ions are shown in Figure 2.3.1, including the respective threshold energies. The total photoionization cross sections and branching ratios are given in

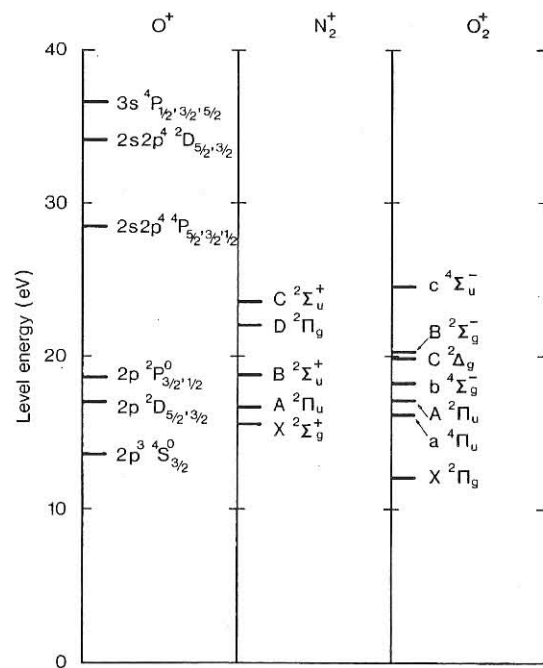


Fig. 2.3.1 Partial energy level diagrams of the major ionizable thermospheric species. The lowest level corresponds to the ionization energy of the neutral species.

Appendix 2, as is the fraction of ionization events going into dissociative ionization. For computational convenience the same wavelength intervals are adopted that have been used for the solar irradiance spectrum and for the absorption cross sections. We will learn in Chapter 7 how several excited states produced by photoionization lead to optical emissions that are part of the dayglow spectrum (Problem 4).

## 2.4 Photodissociation

Photodissociation of  $O_2$  accounts for O being the major neutral species in the thermosphere above about 200 km. Two-body recombination is very slow so that O atoms must diffuse downward into the denser regions of the atmosphere where three-body recombination is the destruction mechanism, i.e., below approximately 100 km. The time constant for downward diffusion of O atoms is long compared with the diurnal cycle of solar illumination, preventing any significant night time decrease in the thermospheric abundance of O atoms.

The dissociation threshold energy of  $O_2$  is only 5.12 eV (Table 2.2.1) so that photons at wavelengths less than 2422 Å are effective in the process

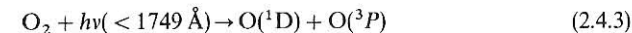


However, solar irradiance beyond 1800 Å is absorbed below the thermosphere and most of the thermospheric dissociation of  $O_2$  is caused by photons in the wavelength region of the Schumann Runge continuum. Taking account of the entire spectral range, the rate of photodissociation at altitude  $z$  is

$$P_z^d(O_2) = n_z(O_2) \int_{2422\text{\AA}}^{650\text{\AA}} I_z(\lambda) \sigma_{O_2}^d(\lambda) d\lambda \quad (\text{cm}^{-3} \text{ s}^{-1}) \quad (2.4.2)$$

where  $\sigma_{O_2}^d(\lambda)$  is the photodissociation cross section. The short wavelength limit of integration, 650 Å, corresponds to the photoionization limit, i.e., photon absorption leads almost entirely to ionization (Appendix 2).

In Section 2.3 we noted that photoionization leads to several electronically excited states of the ions. Photodissociation likewise can lead to excitation of the products.



The excitation energy of the  $O(^1D)$  state is 1.97 eV (see Appendix 3). We mentioned earlier that it is the solar irradiance at wavelengths less than of about 1800 Å that is absorbed by  $O_2$  in the thermosphere. Photodissociation of  $O_2$  in the thermosphere is therefore a copious source of excited O atoms. This has important consequences which will be explored in succeeding chapters.

$N_2$  molecules also photodissociate. However, the process is quite different from dissociation of  $O_2$  which occurs primarily by absorption of continuum radiation.  $N_2$  molecules are first excited into several high lying valence and Rydberg states, called predissociation states which decay largely by dissociation of the molecule instead of by radiation. The absorption bands responsible for this process lie in the wavelength region between about 800 and 1000 Å (Fig. 2.2.2), i.e., just beyond the ionization threshold. Although not the major source of N in the thermosphere, photodissociation of  $N_2$  via excitation of predissociation levels does contribute to the production of this minor constituent. It is generally assumed that the difference between the total

absorption cross section of  $N_2$  and the ionization cross section (Appendix 2) is the effective dissociation cross section that may be used to compute the N atom production rate by an equation similar to Equation (2.4.2) (Problem 5). The predissociation mechanism is described in greater detail in Chapter 4 in connection with electron impact dissociation of  $N_2$ .

## 2.5 Photoelectrons

In our discussion of photoionization (Section 2.3) we indicated by Reactions (2.3.1)–(2.3.3) that the process leads to the production of ion–electron pairs, and this also applies to dissociative ionization, Reactions (2.3.6) and (2.3.7). The threshold wavelengths associated with each reaction specify the minimum photon energy that is required for the reaction to proceed; however, the photoionization cross section is larger at wavelengths shorter than the threshold wavelength (Appendix 2). The reactions, therefore, proceed at a higher rate in association with excess energy. As already mentioned, there is the probability (cross section) that the excess energy leads to internal excitation of the product ions (e.g.,  $N_2^+ A^2\Pi_u$ ,  $O_2^+ a^4\Pi_u$ ,  $O^+ ^2D$ ) but much of the excess energy is channelled into kinetic (translational) energy of the products. Momentum conservation shows that most of the energy is imparted to the lighter electrons. Photoionization, therefore, is a source of energetic photoelectrons. The energy spectrum of photoelectron production is governed by the UV photon flux, a multitude of photoionization cross sections and the neutral gas composition of the atmosphere. The production rate of photoelectrons with energy  $E$  at altitude  $z$  is given by

$$P_z^e(E) = \sum_j \sum_l \sum_\lambda n_z(j) \sigma_j^l(\lambda) p_j^l(l, \lambda_{th}, \lambda) I_z(\lambda) \quad (\text{cm}^{-3} \text{s}^{-1}) \quad (2.5.1)$$

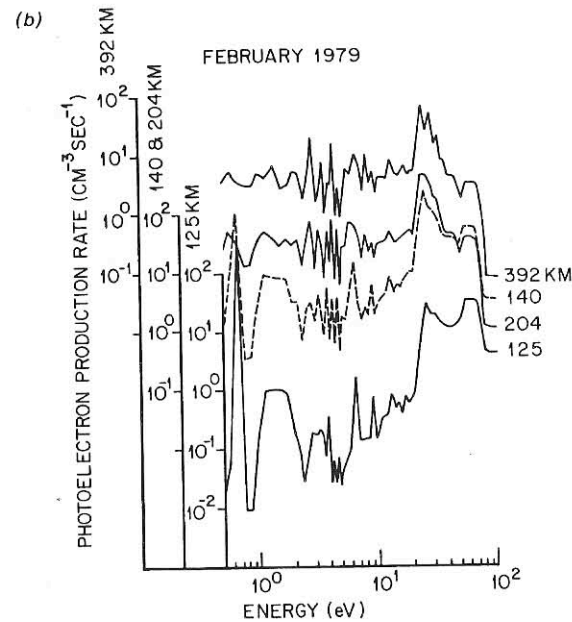
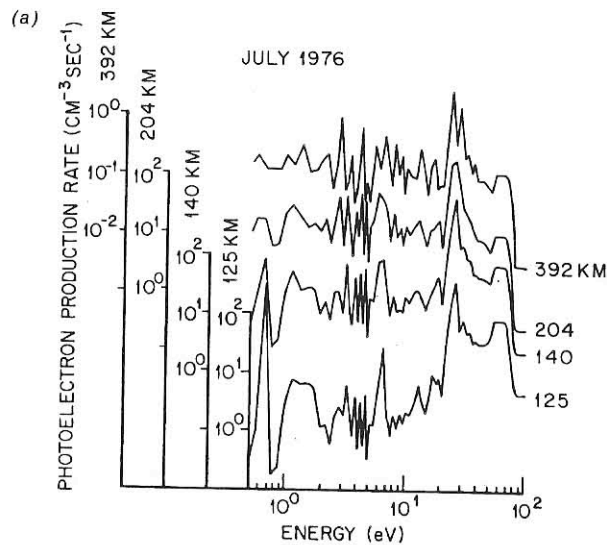


Fig. 2.5.1 The production rate of photoelectrons for typical solar minimum (a) and solar maximum (b) conditions as a function of electron energy at selected altitudes.

The electron energy will henceforth be specified in energy units, with

$$E = hc(1/\lambda_{th}(j, l) - 1/\lambda) \text{ (eV)} \quad (2.5.2)$$

Planck's constant is  $h$  and  $c$  is the speed of light. The threshold wavelength (or energy) is a function of the electronic state,  $l$ , of species,  $j$ . As noted in Section 2.1, the intensity of solar irradiance,  $I_z(\lambda)$ , may be specified per angstrom (Figures 2.1.1 and 2.1.2) or in finite wavelength intervals (e.g. 50 Å) plus discrete emission lines, as in Appendix 2. The summation over  $\lambda$  in Equation (2.5.1) must be treated accordingly. The branching ratios and excitation thresholds for the electronic states of the three major species in the thermosphere are listed in Appendix 2, corresponding to the states shown in Figure 2.3.1. Variability in the solar irradiance,  $I_\infty(\lambda)$ , with solar activity results in a corresponding variation of the photoelectron production rate,  $P_z^e(E)$  (Problem 6). The production rates of photoelectrons as a function of energy for solar minimum (July 1976) and solar maximum (February 1979) conditions are shown in Figure 2.5.1 at selected altitudes. The structure in these curves is a consequence of structure in the solar irradiance as a function of wavelength.

## Bibliography

The solar UV irradiance is one of the fundamental parameters in an investigation of the upper atmosphere and considerable effort has been expended in acquiring measurements of the



absolute fluxes and the variability with solar activity. A recent review paper evaluates published irradiance data from 1350 to 4000 Å:

P.C. Simon and G. Brasseur, Photodissociation effects of solar UV radiation, *Planet. Space Sci.*, **31**, pp. 987–99, 1983.

This paper also discusses the absorption cross section of  $O_2$  which is required to interpret the flux measurements in the wavelength region considered in the review. Over eighty references are given to publications on the solar irradiance and absorption cross sections. The results of irradiance measurements obtained by many investigators over several years are compared, using as reference spectrum the one given in tabular form by

G. Brasseur and P.C. Simon, Stratospheric chemical and thermal response to long-term variability in solar UV irradiance, *J. Geophys. Res.*, **86**, 7343–62, 1981.

A critical evaluation of the solar irradiance between 140 and 1850 Å acquired by the Atmosphere Explorer satellites is given in the paper:

H.E. Hinteregger, K. Fukui, and B.R. Gilson, Observational, reference and model data on solar EUV, from measurements on AE-E, *Geophys. Res. Lett.*, **8**, 1147–50, 1981.

This paper gives references to the sources of the measurements, specifically, the so-called reference spectrum acquired during a rocket flight:

L. Heroux and H.E. Hinteregger, Aeronomical reference spectrum for solar UV below 2000 Å, *J. Geophys. Res.*, **83**, 5305, 1978.

The measurements on which the curves shown in Figures 2.1.2 and 2.1.3 are based are given in the paper

H.E. Hinteregger, Representations of solar EUV fluxes for aeronomical applications, *Adv. Space Res.*, **1**, 39, 1981.

Photoionization and photoabsorption cross sections in the wavelength region 34 Å to 1027 Å are given in a compilation of experimental and theoretical results by

K. Kirby–Docken, E.R. Constantinides, S. Babeu, M. Oppenheimer and G.A. Victor, Photoionization and photoabsorption cross sections of He, O,  $N_2$  and  $O_2$  for aeronomic calculations, *At. Data Nuclear. Data Tables*, **23**, 63–82, 1979.

The above data compilation also gives the branching ratios into excited states of O,  $N_2$  and  $O_2$  and the dissociative ionization yield for the molecular species. In the longer wavelength region absorption cross sections are summarized in the review article

K. Watanabe, Ultraviolet absorption processes in the upper atmosphere, *Adv. in Geophys.*, **5**, 153, 1958.

The density and composition of the neutral atmosphere may be specified by empirical models, based on very large data sets acquired by satellite borne instruments and ground based measurements. One such model includes data compiled over many years' observations, allowing for different levels of solar activity, magnetic activity, geographic and diurnal variations:

A.E. Hedin, MSIS-86 thermospheric model, *J. Geophys. Res.*, **92**, 4649, 1986.

The above cited paper gives references to preceding publications on empirical model atmospheres.

## Problems 1–6

**Problem 1** Identify some prominent line emissions in the solar spectra shown in Figures 2.1.1 and 2.1.2. Use the tables in Appendix 2 as well as the references. Which lines show large differences in intensity between solar minimum and maximum conditions?

**Problem 2** Derive Equation (2.2.5) for the optical depth for solar zenith angles greater than  $90^\circ$ .

**Problem 3** Compute the altitude at which  $I(\lambda)$  is reduced to  $1/e$  of the irradiance at the top of the atmosphere,  $I_\infty(\lambda)$ , as a function of wavelength for a solar zenith angle of  $40^\circ$ . Use the absorption cross sections in Appendix 2.

**Problem 4** Compute the photoionization rate for solar maximum conditions when the solar zenith angle is  $40^\circ$ . Compute the altitude profiles of the production rate of various ions of the major thermospheric species. Assume that ions produced by dissociative ionization are formed in the ground state.

**Problem 5** Compute the N atom production rate as a function of altitude by photodissociation of  $N_2$  for solar maximum conditions and a solar zenith angle of  $40^\circ$ .

**Problem 6** How much energy does a photoelectron acquire when produced by HeI photons ionizing  $N_2$ ? Compute the photoelectron production rate due to the HeI and HeII solar emission lines at 170 km altitude for day 113 in 1974 and day 50 in 1979 for a solar zenith angle of  $40^\circ$ .